ELSEVIER

Applied Catalysis A: General 198 (2000) 115–126

APPLIED CATALYSIS A: GENERAL

www.elsevier.com/locate/apcata

In-situ study of MCM-41-supported iron oxide catalysts by XANES and EXAFS

She-Tin Wong [a], Jyh-Fu Lee [b], Soofin Cheng [a], Chung-Yuan Mou [a,*]

[a] *Department of Chemistry, National Taiwan University, 1, Roosevelt Road Section 4, Taipei, Taiwan*

[b] *Synchrotron Radiation Research Center, Hsinchu, Taiwan*

Received 24 August 1999; received in revised form 24 November 1999; accepted 24 November 1999

Abstract

Our study focuses on the structural evolution of MCM-41-supported iron oxide under the reducing environment of catalyst pretreatment and ethylbenzene dehydrogenation reaction. Powder X-ray diffraction (XRD) analysis showed that the iron oxide is well-dispersed on the surface of the support with no detectable diffraction peaks from iron oxide. X-ray absorption near edge structure (XANES) study indicates that iron oxide is being reduced during catalyst pretreatment under flowing helium from α-Fe_2O_3 at room temperature to Fe_3O_4 at 425°C. At 500°C, the oxide species is reduced even further. Curve-fitting analysis of the extended X-ray absorption fine structure (EXAFS) radial distribution function (RDF) profile of the catalyst pretreated at 500°C can be done with a basic tetragonal γ-Fe_2O_3 spinel structure. However, the cationic vacancies of the spinel on the octahedral position are almost filled with iron cations, indicating that the structure of the iron oxide species is approaching that of a ccp FeO. Stabilization of the FeO-like structure formed at 500°C is probably through iron oxide-support interactions, especially via condensation of the oxide terminal hydroxyl groups with the silanols of MCM-41. This distorted form of iron oxide species is metastable and contains labile surface oxide anions, which are probably responsible for the high initial catalytic activity during ethylbenzene dehydrogenation reaction at 500°C. In the presence of the reactant, however, the iron oxide is further reduced and metallic iron is formed during the reaction. The formation of metallic iron is probably through fragmentation of FeO particles, as shown by catalysis and EXAFS results. The reduction process contributes mainly to the deactivation of the catalyst.

Keywords: MCM-41; Iron oxide; XANES; EXAFS; Ethylbenzene dehydrogenation

1. Introduction

In heterogeneous catalysis, the knowledge of catalyst structure is essential in order to understand the chemistry actually occurring on the surface of a catalyst. This makes structure characterization crucial throughout the life cycle of the catalyst, from the preparation step to the use in catalytic reaction. However, the majority of these studies were carried out in an ex-situ manner where the conditions of the catalyst are far from those generally present in a catalytic reactor. Besides, the phase composition and the texture of the catalyst may change under the reaction conditions, especially when the reaction temperature is very high. Some studies have shown that static surface structures and reaction mechanisms in vacuo are generally different from dynamic ones under reaction

* Corresponding author. Fax: +886-2-2366-0954.
E-mail address: cymou@ms.cc.ntu.edu.tw (C.-Y. Mou)

0926-860X/00/$ – see front matter
PII: S0926-860X(99)00516-5

conditions [1–5]. Thus, in-situ study has become increasingly important, since the real chemistry of the surface can only be understood by approaching the real reaction condition as much as possible.

In the last two decades, due to the significant improvement of instrumentation and computer power, the easier access to synchrotron radiation sources and the development of powerful software for structural modeling, it is possible to carry out structural analysis on well-dispersed catalysts using X-ray absorption techniques such as X-ray absorption near edge structure (XANES) and extended X-ray absorption fine structure (EXAFS) [6,7]. This evolution is of paramount importance for a supported metal or metal oxide catalyst, since the active phase of an efficient catalyst mostly exists in the form of highly dispersed state on high surface area supports. In this regard, the main advantage of X-ray absorption spectroscopy over other techniques is that it provides direct information on charge density and the local environment of a specific absorbing atom without the requirement of long-range ordered structure and UHV conditions.

In this paper, we apply the XANES and EXAFS techniques to an in-situ study of ethylbenzene dehydrogenation on iron oxide catalyst. EXAFS techniques have been used to study the catalyst system in ethylbenzene dehydrogenation reaction but not in an in-situ manner [8]. Moreover, the catalyst system studied was too complicated.

The nature of the reaction centers for ethylbenzene dehydrogenation is still a matter of controversy. Numerous models have been put forward, which is reasonable considering the vast number of catalyst systems and experimental conditions studied. Among these models, two are of particular interest to us. The first one involves $KFeO_2$ as the active phase as proposed by Hirano [9]. However, we believe that the involvement of crystalline $KFeO_2$ phase in the reaction process is not very likely since the direct synthesis of $KFeO_2$ requires a much higher temperature (1000°C) than the usual reaction temperature of ethylbenzene dehydrogenation (550–600°C). Another interesting model is suggested by Koppe et al. [10], involving potassium-doped γ-Fe_2O_3 as the active ingredient. Here, the incorporation of potassium ions in the γ-Fe_2O_3 lattice sites leads to a defective γ-Fe_2O_3 structure. In general, all the models proposed in the study of ethylbenzene dehydrogenation point toward the importance of a K–O–Fe^{3+} entity as the active center of the catalyst.

As in the case of other related studies, the primary goal of this study is aimed at unveiling the problem of the active center(s) involved in the ethylbenzene dehydrogenation reaction. However, our basic approach is to simplify the reaction system as much as possible, i.e. using an unpromoted catalyst and without the cofeeding steam in the reactant. The basis of our consideration is that the promoter such as the potassium species used in the industrial catalysts only modifies but does not alter the nature of the active center, e.g. the electronic density of iron center may have changed, giving rise to an improved catalytic activity and styrene selectivity. In fact, literature studies have shown that the active centers are the same for the promoted and unpromoted catalysts [11,12]. But the steam in the reaction stream only functions as a diluent and catalyst regenerating agent [13]. The absence of steam will thus allow us to follow the catalyst deactivation process more easily.

We are also interested in the study of supported catalyst systems. It is known that MCM-41 has high surface area and porosity [14], so it is possible to use it as a support for preparing highly dispersed metal or metal oxide catalysts. A direct strategy in catalyst preparation is to use the mesoporous silica as a host for reactive chemical species through the deposition or impregnation of various organometallic precursors. In addition, the surface of MCM-41 contains an abundant supply of silanol groups; therefore, a wide variety of stable and surface-anchored species can be made successfully by this method via the surface reaction with the silanol groups on the wall of the MCM-41 channels. Some of the MCM-41 supported species have been claimed to display high catalytic activities [15]. On the other hand, there is very limited work in elucidating the structures of these MCM-41 supported species, particularly so in an attempt to correlate the structures with their catalytic activities.

In this paper, we show that XANES and EXAFS analysis of the MCM-41 supported iron oxide catalysts can provide structural information on the surface-attached Fe–O species. From the proposed structural model, active site(s) for ethylbenzene dehydrogenation reaction is proposed. Special interest has been focused on correlating the ethylbenzene dehydrogenation activity and the mobility of iron cations

in iron oxide, particularly so in the case of Fe_3O_4 spinel. A detailed discussion of the catalyst system and catalytic performance is the subject of another publication, but information related to this study is included in Section 3 [16].

2. Experimental

2.1. Catalyst preparation and characterization

The method used for the synthesis of MCM-41 was adapted from our published literature [17]. MCM-41-supported catalysts were prepared by impregnating the MCM-41 support with an aqueous solution of ammonium iron(III) oxalate trihydrate, $(NH_4)_3Fe(C_2O_4)_3{\cdot}3H_2O$, or ammonium heptamolybdate, $(NH_4)_6Mo_7O_{24}{\cdot}4H_2O$. After being dried at 100°C, the samples were calcined at 500°C for 6 h. All the catalysts used in this study have a metal loading of 6 wt.%.

The catalyst and support were characterized with various techniques such as powder X-ray diffraction (XRD), surface area and pore size measurements, and we found that the catalyst retained much of the periodic nano-structure of the pristine MCM-41.

2.2. Catalytic reaction

Reactions were carried out in a continuous flow micro-reactor system at atmospheric pressure. The reactant, ethylbenzene, was injected continuously ($2.72\,ml\,h^{-1}$) into the nitrogen carrier gas stream (effluent flow rate=$30\,ml\,min^{-1}$) and the reaction product (gas and liquid) was analyzed off-lined by a Shimadzu GC-7A gas chromatograph. Liquid product was collected by a condenser (10°C) positioned at the outlet of the reactor and the components were separated with a packed column (5% SP-1200+1.75% Bentone 34 on 100/120 Suplecoport, 6 ft). Catalyst regeneration was done at 500°C under an air flow of about $75\,ml\,min^{-1}$ for 1 day (iron sample) or 6 h (molybdenum sample). The amount of carbon left on the catalyst surface after the reaction was determined with a Perkin–Elmer CHN-2400 elemental analyzer.

Total conversion of ethylbenzene is defined as the percentage of ethylbenzene converted to hydrocarbon products. The products are light hydrocarbons, benzene, toluene, styrene and polyaromatic compounds such as dimers and trimers of styrene. Styrene selectivity is defined as the percentage of styrene in the observed product. Both the conversion and selectivity data were based on the amount of carbon.

2.3. XANES and EXAFS studies

2.3.1. X-ray absorption measurements

X-ray absorption measurements were carried out with synchrotron radiation using the EXAFS facilities installed at the Synchrotron Radiation Research Center, Hsinchu, Taiwan. The storage ring was operated at about 1.5 GeV with about 200 mA ring current. For the in-situ experiment, finely powdered sample was pressed into pellet ($\leq$1 mm thick) and sat within a sample holder. The temperature of the pellet can be varied by changing the temperature of a home-made in-situ cell. The carrier gas used is helium, which was bubbled through an ethylbenzene reservoir at a flow rate of about $30\,ml\,min^{-1}$. The data for ex-situ experiment was recorded at room temperature with the sample uniformly spread onto a strip of adhesive tape, which was then folded into two layers to obtain an optimum absorption jump ($\Delta\mu t \approx 1$) enough to be free from thickness and pinhole effects [18]. All the data were recorded in transmission mode using an Si (1 1 1) channel-cut monochromator. Intensities of the incident and transmitted beams were measured in ionization chambers filled with a gas mixture of higher density.

2.3.2. Data analyses

All the experimental spectra were analyzed with a standard procedure similar to those outlined in [18]. The threshold energy (E_0) of α-Fe_2O_3 determined at half-height of the absorption edge jump (1s$\rightarrow$4s transition) was 7123.2 eV, which is in close agreement with 7126.4 eV reported by Sankar et al. [19]. The resulting EXAFS spectra were k^3-weighted in order to compensate for the attenuation of EXAFS amplitude at high k and then Fourier transformed in the range of about $2.55\,Å^{-1} \leq k \leq 11.5\,Å^{-1}$ with a Hanning apodization function of $dk=2\,Å^{-1}$.

To avoid the unnecessary computations in the course of EXAFS fitting of the experimental spectrum

(using FEFFIT program version 2.32), the coordination number (N) was fixed to the crystallographic value of known compounds and the amplitude reduction factor (S_0^2) was set equal to 0.9 for all compounds [18]. We also varied the mean square displacement of path distance or Debye–Waller Factor (σ_i^2) and the threshold energy difference (ΔE_0) for all paths in order to optimize the fit of the theoretical data to the experimental data. However, the magnitude of σ_i^2 was constrained to reasonable values by referring to the published results on σ^2 versus temperature relationship by Yokoyama et al. [20]. The hypothetical structure used in the fitting process was obtained from the published results of Shmakov et al. [21]. In this case, the atomic coordinates of a basic cubic spinel-like unit cell of γ-Fe_2O_3 were fitted with a tetragonal space group (Hermann–Maguin Notation: P 41 21 2) rather than the reported cubic space group (P 43 3 2). Nevertheless, a tetragonal basic unit cell of γ-Fe_2O_3 has been reported by Greaves [22] with lattice constants a=8.3396 Å and c=8.3221 Å.

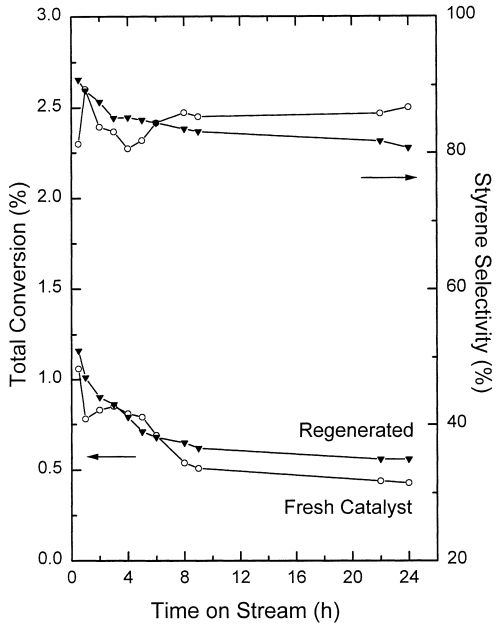

Fig. 1. Catalytic performance of MCM-41-supported iron oxide catalysts at 500°C.

3. Results

3.1. Catalytic system

MCM-41 was chosen as the catalyst support because of its high surface area (1100 $m^2\,g^{-1}$), which enables a better dispersion of catalytic active materials. In our MCM-41-supported iron oxide catalyst, for example, iron oxide is highly dispersed on MCM-41 surfaces since no XRD peaks other than the pristine MCM-41 are observed. The persistence of the MCM-41 diffraction peaks indicates that the structure of MCM-41 remained intact during the catalyst preparation process. The catalyst still retained much of the surface area (774 $m^2\,g^{-1}$) of MCM-41, but the porosity of the catalyst is significantly lower (from 0.93 to 0.53 ml g^{-1}). Since the catalyst loading is only 6 wt.%, the decrease in porosity should be due to the partial collapse of the uni-dimensional channels of MCM-41.

We have previously studied a series of MCM-41-supported molybdenum oxide and iron oxide catalysts in ethylbenzene dehydrogenation reaction. Depending on the method of catalyst preparation, large surface area MCM-41 supported catalysts can have 1.5–2.4 times increases in steady state activity over amorphous silica supported ones (surface area=377 $m^2\,g^{-1}$). We also found that molybdenum-based catalyst is about 3.3 times higher in steady state activity than iron-based catalyst. On the other hand, the selectivity of styrene, which is the major product, is comparable (93% versus 87%). However, due to the limitation of our synchrotron source energy, we are not able to carry out X-ray absorption study on molybdenum samples, hence, only the results for iron catalysts are presented.

Fig. 1 shows the catalytic performance of both fresh and regenerated MCM-41-supported iron oxide catalysts in the ethylbenzene dehydrogenation reaction. The activity of the catalyst is high initially, but decays at increasing time on stream to a steady state value. It is possible that different active centers are involved in the initial and steady stages of reaction. We also found that the activity profile of the fresh catalyst fluctuates during the initial period of reaction. This is not an experimental artifact, since a similar but opposite trend is also observed for styrene selectivity. A possible explanation is the fragmentation of large iron oxide particles into smaller micro-particles via a reductive

process. The participation of fresh active centers on the newly exposed surface has an added effect on the reaction activity. On the other hand, the styrene selectivity varies inversely with activity since a more active surface tends to catalyze more secondary reactions (refer to the first selectivity data). Secondary reactions include styrene or ethylbenzene cracking (giving benzene, toluene and light hydrocarbon) and styrene oligomerization. The styrene selectivity finally stabilized at ≈87% after the fragmentation process was completed. This behavior diminished in the regenerated catalyst due to improved dispersion of iron oxide after a reduction–oxidation cycle. Now, the particle size of iron oxide must be small and the activity and styrene selectivity will decrease monotonously with time on stream due to catalyst deactivation.

Larger fluctuations in activity are also observed over fresh MCM-41-supported molybdenum oxide catalyst, but at a lower reaction temperature of 400°C. Here, the styrene selectivity was even lower initially (≈23%), indicating the abundance of cracking and oligomerization products, but finally stabilized at ≈93% within 3 h of reaction. When the reaction was carried out at 500°C, the reductive disintegration process was too fast to be observed.

The reliability of the X-ray in-situ cell in ethylbenzene dehydrogenation reaction was also checked. A much higher conversion of ethylbenzene (up to about 10-fold) than the catalytic micro-reactor was obtained especially during the initial stages of reaction while the styrene selectivity was comparable. It should be emphasized that the design of the catalytic micro-reactor is completely different from that of the in-situ cell so that direct quantitative comparison of results should be avoided. Only qualitative comparison should be envisaged.

In this paper, we try to provide results from X-ray absorption studies related to the two phenomena observed in our catalytic dehydrogenation reaction: (i) the nature of active sites involved in the initial and steady states of reaction; (ii) reductive disintegration of iron oxide during the process of reaction. Since both of them are continuous processes, and in order to avoid contamination, we carried out our study in an in-situ manner. Besides, X-ray absorption techniques can also provide us direct information on the structural evolution of iron oxide at various temperatures.

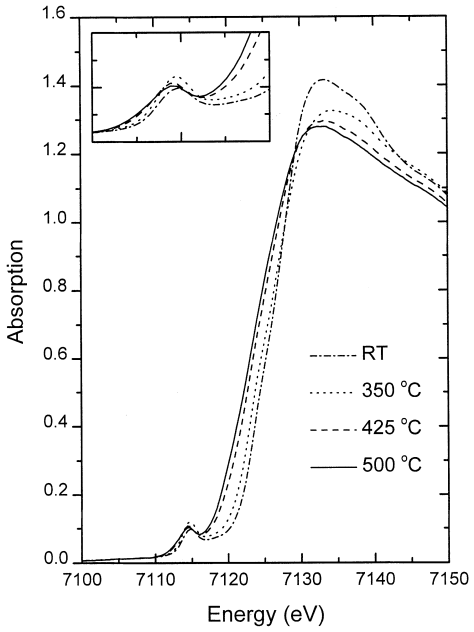

Fig. 2. Fe K-edge XANES spectra of MCM-41-supported iron oxide catalyst pretreated at different temperatures.

3.2. Carbon analysis

The carbon content of the catalyst sample after the in-situ X-ray absorption study was also analyzed. The amount of carbon left on the surface is less than 1.6 wt.% which corresponds to nearly 1.2 atoms of carbon per atom of iron. A comparable value was also obtained in the actual catalytic run.

3.3. XANES study

In Fig. 2, we present a typical iron K-edge XANES spectra of MCM-41-supported iron oxide catalyst pretreated at various temperatures. For the purpose of comparison, these spectra were recorded after the sample was maintained at similar time intervals (<0.5 h) at each temperature. As the pretreatment temperature of the catalyst rises, the absorption edge shifts progressively towards lower absorption energy. With reference to the standard compounds, we found that the iron oxide in the as-synthesized catalyst (at room temperature) has a nature similar to that of α-Fe_2O_3, while at 425°C, Fe_3O_4 is a more likely candidate. The absorption spectrum and its first derivative of our

α-Fe_2O_3-like sample are also similar to those of bulk α-Fe_2O_3 reported by Grunes [23]. The insert of Fig. 2 shows an expanded pre-edge region where the spectral changes are also consistent with structural transformation from α-Fe_2O_3-like to Fe_3O_4-like. Formally, this 1s→3d electric-dipole transition is Laporte forbidden, but it gains intensity through coupling mechanisms such as direct quadrupole coupling or vibronically allowed dipole coupling [24,25]. This transition gains additional intensity when the iron center is in a non-centrosymmetric environment or through mixing of iron 3d orbitals with 4p ones. We would then expect that tetrahedrally coordinated iron compounds show more intense pre-edge peak than those coordinated octahedrally. Peak broadening is also observed and the peak maximum shifted slightly to lower absorption energy, which can be explained by the presence of an additional octahedrally coordinated Fe^{2+} species in the Fe_3O_4 inverse spinel.

The iron K-edge XANES spectra of the catalyst after ethylbenzene dehydrogenation reaction at 500°C were analyzed as well (figures not shown). It is not very surprising to observe further reduction of the catalyst during the reaction, but it seems that the reduction process is not a continuous one, since it takes place only in a very short period of time (a few minutes) during the initial stages of reaction. At the same time, the main pre-edge peak almost disappeared, while the low energy shoulder became more prominent. Possibly, some α-Fe is formed at this stage. Clearly, not all the lattice oxygen are easily removed at this temperature.

3.4. EXAFS study

The radial distribution function (RDF) profiles of the experimental iron K-edge EXAFS spectra of the catalyst pretreated at various temperatures are presented in Fig. 3. The conditions of these spectra correspond to the XANES spectra in Fig. 2. Some of the selected results from curve-fitting analysis of the various coordination shells of octahedral iron center are listed in Table 1. The first peak of the RDF profile is asymmetric, and thus, two shells were considered in the fitting process instead of one (oxygen neighbors). Also, the third, fourth and fifth peaks of as-synthesized catalyst were assigned to face-, edge- and vertex-sharing FeO_6 octahedra, respectively, according to the published bond distances of α-Fe_2O_3 (iron neighbors) [26]. However, one should note that the structure of iron oxide varies with temperature, so that these assignments should not be taken rigorously for high temperature-treated samples. Other structural information on α-Fe_2O_3 and related oxides can be found in [27,28].

A closer look at the relationship between peak intensity and pretreatment temperature revealed some interesting phenomena. While the intensity of the first peak decreases monotonously with increasing temperature, the reverse is observed in the second peak which maximized at 500°C. Although both peaks were assigned to oxygen neighbors (Fe–O), they ought to have different origins: the oxygen neighbors of iron in the bulk and on the surface, for example. Also, as the

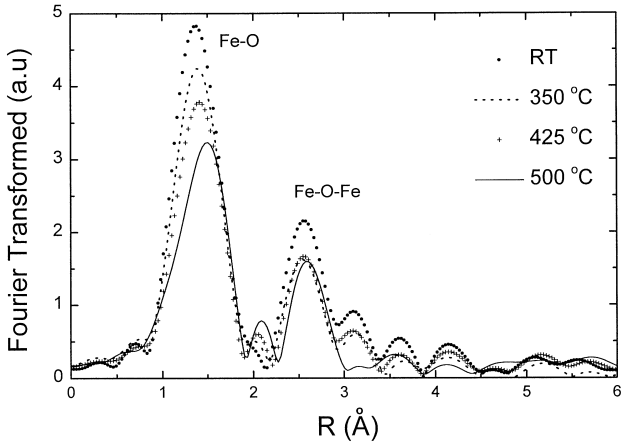

Fig. 3. Fe K-edge EXAFS RDFs of MCM-41-supported iron oxide catalyst pretreated at different temperatures.

Table 1
EXAFS curve-fitting data of various iron oxide samples[a]

Sample	N	N	R	R
			σ^2	σ^2
	Fe–O	Fe–O–Fe	Fe–O	Fe–O–Fe
α-Fe_2O_3	(3.0)(3.0)	(1.0)(3.0)(3.0)	(1.925)(2.053) (0.008)(0.008)	(3.034)(2.989)(3.504) (0.040)(0.002)(0.003)
A	(3.0)(1.4)	(1.0)(2.2)(0.3)	(1.900)(2.028) (0.008)(0.008)	(2.774)(3.019)(3.451) (0.040)(0.013)(0.003)
B	(4.0)(1.6)(5.2)	(11.8)	(2.062)(2.104)(2.133) (0.016)(0.016)(0.015)	(2.956) (0.015)
C	(3.5)	(1.9)	(1.972) (0.016)	(2.908) (0.015)

[a] N=coordination number, R=bond length (Å). A: as-synthesized catalyst purges with He at room temperature. Both α-Fe_2O_3 and this sample were treated with corundum model in the fitting process. B: sample A pretreated under flowing He at 500°C (treated with distorted spinel model). C: sample A pretreated under flowing He at 500°C (treated with cubic spinel model).

temperature increased, the third peak stopped diminishing at 425°C, supporting the XANES observation of a structural transformation of α-Fe_2O_3 to Fe_3O_4 at this temperature. The third and fourth peaks should now correspond to the octahedral and tetrahedral iron neighbors in the spinel. It should be mentioned again that α-Fe_2O_3 has a corundum structure, while Fe_3O_4 has an inverse spinel structure. A new peak emerged at about the same R-value (but probably of different origin) as the vertex-sharing iron neighbor in the as-synthesized catalyst. Peaks at even higher R-values due to more distant coordination shells are not treated, since they are complicated by severe and complex overlapping of single and multiple scattering phenomena [18]. At 500°C, the fourth peak due to tetrahedral iron neighbor diminished.

These RDF profiles were further simulated following a standard curve-fitting analysis procedure; the case at 500°C is shown in Fig. 4. A very good fit is observed between the experimental and simulated profiles using a tetragonally distorted spinel structure as the hypothetical model. The best fit to the experimental profile has an r-factor of fit of 0.05 in the R-range of $0.12 \leq R$ (Å) ≤ 2.95 which is better than or comparable to those of Kou et al. [29]. Unexpectedly, a much poorer fit is obtained with undistorted cubic spinel structure as the hypothetical model (r-factor=0.25). A similar result was obtained with sodium chloride structure (r-factor=0.18). In addition, the second peak in the latter two cases cannot be resolved in the fitted spectrum. Also, the RDF profiles of bulk α-Fe_2O_3 and as-synthesized catalyst were fitted with corundum structure and the r-factors are 0.06 and 0.05 ($0.12 \leq R$ (Å) ≤ 4.0), respectively.

Table 1 gives a summary of the selected curve-fitting results of this study. In the as-synthesized catalyst, the iron center of α-Fe_2O_3 is slightly coordinatively unsaturated as shown by the loss of the vertex-sharing iron

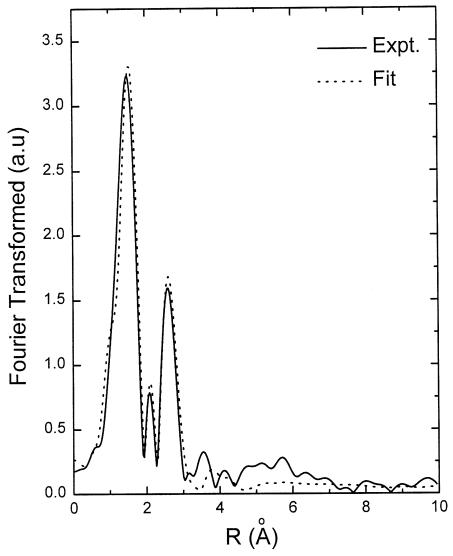

Fig. 4. The best fit to the Fe K-edge EXAFS RDF of MCM-41-supported iron oxide catalyst pretreated at 500°C.

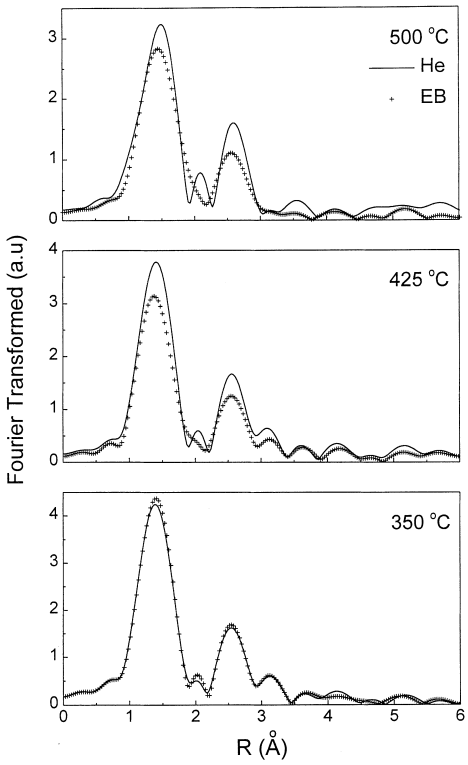

Fig. 5. Comparison of the Fe K-edge EXAFS RDFs of MCM-41-supported iron oxide catalyst before and after the ethylbenzene dehydrogenation reaction at three different temperatures.

neighbor. The corresponding interlayer face-sharing iron neighbor remained intact, probably due to strong bonding interactions between the two octahedral units. These neighbors resist the spreading of iron oxide during the calcination process of catalyst preparation.

Fig. 5 compares the RDF profiles of the catalyst at three different temperatures before and after reacting with ethylbenzene. The spectra at 350 and 425°C were recorded after about 1 h of reaction, but they was recorded immediately at 500°C to avoid excessive coke formation. Clearly, the reaction begins at temperatures above 350°C where the decrease in the intensity of the Fe–O and Fe–O–Fe coordination peak is quite significant. Special notice should be put on the small peak (surface Fe–O coordination) which seems to grow in larger proportion after interacting with ethylbenzene at a temperature of 350°C, during which practically no reaction or reduction occurs.

The nature of the catalyst was also followed at different times on stream (figures not shown). When the catalyst is in contact with ethylbenzene, shoulders start to develop beside the Fe–O and Fe–O–Fe coordination peaks and the latter seems to increase with reaction time. Comparing with the profile of a highly hydrogen reduced Fe/TiO_2 sample prepared by Kou et al. [29] shows that metallic α-Fe is developed at this stage. In a heavily coked sample, these shoulders become very prominent.

4. Discussion

From the point of view of heterogeneous catalysis, it is always advantageous to have the catalytically active phase (such as iron oxide in our case) highly dispersed on a support, since the increased number of active sites will surely lead to an increase in catalytic activity. However, extracting structural information from these iron oxides in a highly dispersed state by using the common structural elucidation techniques is not an easy task, since they usually lack long-range ordered structure. Fortunately, there exist powerful local probes such as XANES and EXAFS techniques from which valuable and interesting information regarding the chemical environment of supported iron oxide catalyst can be derived.

The method of catalyst preparation followed that of Gao et al. [30], which produced α-Fe_2O_3 on the surface of the as-synthesized catalyst. Iron K-edge EXAFS study gave a detailed picture on the structural geometry of this surface α-Fe_2O_3 with corundum structure. Preliminary examination of the as-synthesized catalyst revealed that partial spreading of α-Fe_2O_3 may have occurred on MCM-41 surface. A large decrease in the number of interlayer vertex-sharing FeO_6 octahedra is observed in the catalyst compared to bulk α-Fe_2O_3 while the interlayer face-sharing and intralayer edge-sharing octahedra in the structure remained largely intact. The dispersed phase of α-Fe_2O_3 may exist mainly in the form of monolayer or bilayer on MCM-41 surface; this suggestion is supported by the absence of XRD peaks of α-Fe_2O_3.

In catalysis, one always pays more attention to the study of the structural evolution of catalyst during reaction rather than during catalyst pretreatment. In extreme cases, the structure and stoichiometry of the

active phase in the catalyst are assumed as invariant properties in the latter process. As shown in Fig. 2, the pre-edge and XANES results of the supported iron oxide catalyst show conclusively that α-Fe_2O_3 is partially reduced even during the pretreatment stages. Hence, the structure and stoichiometry of the active phase on a catalyst can change according to the working environment, a fact that is sometimes ignored in some of the literature works when designing a catalyst system or correlating catalyst performance with structural data.

We use a hypothetical spinel structure as shown in Fig. 6 to demonstrate the process of reduction when the temperature was increased from 425 to 500°C. Only the representative segments of the large unit cell of Fe_3O_4 spinel are presented. Both the tetrahedral and the octahedral iron sites are indicated. The oxide

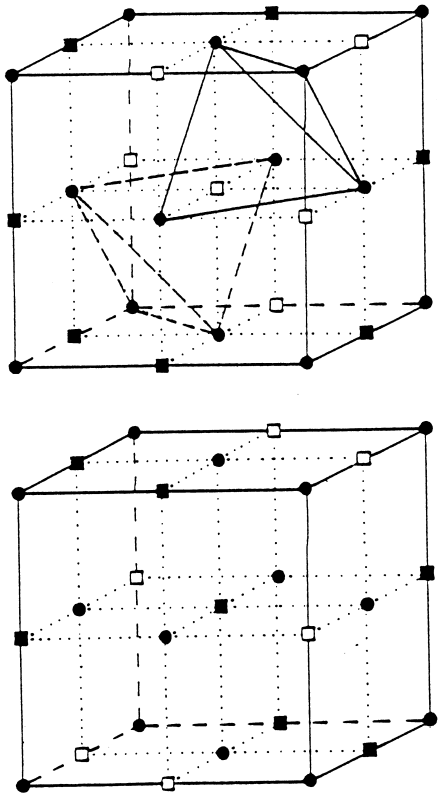

Fig. 6. Representative segments of a unit cell of Fe_3O_4 spinel. Circle symbol: oxygen site, square symbol: octahedral iron site (solid: filled, open: vacant). The tetrahedral irons are shown in the upper diagram where Fe(III) would partially occupy.

Fe_3O_4 is closely related to FeO, all having a cubic unit cell of edge approximately 8.5 Å containing 32 cubic close packed (ccp) oxygen atoms. In FeO, there are 32 octahedral Fe^{2+}, whereas in Fe_3O_4, there are eight octahedral Fe^{2+} together with 16 Fe^{3+} distributed evenly in both octahedral and tetrahedral sites [31]. Accordingly, these phases are easily inter-convertible. The reduction of $Fe_3O_4 \rightarrow FeO$ may be visualized as the continuous removal of outermost cp layers of oxygen atoms accompanied by the migration of iron cations into the octahedral sites in the bulk. The reduction also results in the contraction of the oxygen lattice of Fe_3O_4. A similar mechanism describing the reduction of γ-$Fe_2O_3 \rightarrow Fe_3O_4$ has been proposed by Sakata et al. [32]. Migration of iron cations during the oxidation–reduction process of iron oxide was also detected by other spectroscopic techniques [33,34]. The Auger results revealed that, at temperatures greater than about 302–327°C, iron migration in Fe_3O_4 occurs readily and results in a phase transition from Fe_3O_4 to FeO [33]. Similarly, the overlayer iron atoms were found to dissolve into the nickel crystal bulk at temperature >327°C [34].

Since our reaction temperature is 500°C, it is not very surprising if the true catalytically active iron oxide species involved in the initial period of reaction has a structure intermediate between Fe_3O_4 and FeO. Besides, FeO is not stable at temperatures below 570°C and it will decompose into Fe_3O_4 and α-Fe [31]. However, the structure of iron oxide at 500°C derived from curve-fitting analysis with a distorted spinel model (Table 1, sample B) is more similar to FeO, which has a total of about six nearest oxygen neighbors (first and second coordination shells) and 12 nearest irons (fourth coordination shell) around the octahedrally coordinated iron center. As mentioned before, all the irons in FeO occupy the octahedral sites. The Fe–O and Fe–O–Fe distances are consistent with the reported experimental and theoretical values [18,29,35]. The amount of residual Fe_3O_4 at this stage is probably small, judging from the absence of any prominent peak corresponding to tetrahedral iron which should appear at a slightly longer distance than the octahedral iron in FeO. If a non-distorted cubic spinel is used as the hypothetical structure for curve-fitting analysis, a much poorer fit is observed and the number of oxygen neighbors is unreasonably low for a ccp array of oxide anions (Table 1, sample C). Anyway, a similar

N value for the nearest oxygen neighbors has also been reported by Kou et al. [29] for hydrogen reduced Fe/TiO_2 catalyst. The cause of the tetragonal distortion of FeO at 500°C is not known for sure, but both the Jahn–Teller effect [27,36] and the effect of iron oxide–support interactions will certainly play a role.

In a supported catalyst, the FeO structure must be stabilized by interacting with the MCM-41 surface such as the silanol groups to form Fe–O–Si linkages. We are unable to tell specifically when these linkages are formed, but the presence of hydroxyls on iron oxide has been reported [37]. It should also be mentioned that a new peak starts to emerge at temperatures above 350°C in the EXAFS RDF profile with about the same *R* as the vertex-sharing octahedra of α-Fe_2O_3. With reference to the reported Mn–O–Si distance for MCM-41 supported manganese catalysts [15], this peak is tentatively assigned to Fe–O–Si linkages.

The origin of the small peak (third coordination shell) which appeared in the RDF profiles at a slightly larger *R*-value than the six nearest oxygen neighbors needs some attention. It is unlikely to come from the nearest oxygen neighbors in the FeO_4 tetrahedra since the *R*-values will be slightly smaller than the case in FeO_6 octahedra [21,38]. It is also unlikely to be caused by the close encounter of two nearest iron cations occupying both octahedral and tetrahedral sites, i.e. the tetrahedral iron positions in the original Fe_3O_4 spinel still persist in the newly formed cubic-like structure, a situation which could happen during the reduction of iron oxide. However, besides the stabilization energy requirement, this idea is also discarded since the peak height of this species was found to decrease in the presence of ethylbenzene. After careful consideration, we finally assigned it to distorted Fe–O linkages present on the surfaces of iron oxide. This kind of distortion probably allows the surface Fe–O to maintain a more stable energy state. Consequently, these activated or labile oxide anions of longer bond length (weaker bond strength) can be the primary species responsible for the catalytic activity during the initial stages of the ethylbenzene dehydrogenation reaction. In fact, surface lattice oxygen of γ-Fe_2O_3 has also been found to be involved in the oxidative dehydrogenation of butenes [39].

In the ethylbenzene dehydrogenation reaction at 500°C, the high initial catalytic activity is probably related to the concentration of the labile lattice oxygen. The supply of this species depends on the continual diffusion of surface iron cations into the bulk as the iron oxide is being reduced by ethylbenzene. However, it seems that the reduction of iron oxide, and hence, the supply of labile lattice oxygen, diminished within about 10 min of reaction and this might correspond to the complete filling of cationic vacancies in the bulk. The catalyst thus deactivates unless fragmentation of iron oxide particles can occur (see below). Hence, ethylbenzene dehydrogenation in the initial stages of reaction seems to occur via an oxidative mechanism similar to that proposed by Jebarathinam et al. [40]. Here, the source of oxygen is the surface lattice oxygen and they are removed as water. The stronger Fe–O bonding, such as those present at steady state, can also become involved in dehydrogenation, but via the non-oxidative mechanism described by Chen et al. [41] with hydrogen as the by-product. We suggest that the Fe–O bonding of iron oxide has a distribution of strength, and thus, dehydrogenation ability. In summary, the overall process of ethylbenzene dehydrogenation over supported iron oxide catalyst thus comprises a combination of oxidative (initial stage) and non-oxidative (steady state) mechanisms.

We ascribed the fluctuation of activity in Fig. 1 to the reductive fragmentation of large iron oxide particles. We have mentioned before that FeO tends to decompose into Fe_3O_4 and α-Fe at temperatures below 570°C. The presence of α-Fe is indicated by a shoulder beside the main Fe–O peak at about 2.44 Å in the RDF profile. α-Fe has been known to give a peak at 2.48 Å [29]. The newly formed Fe_3O_4 can provide fresh surfaces for the reaction, as mentioned in the catalytic section (Section 3). The decreased peak height of both Fe–O and Fe–O–Fe coordination in the RDF profile after the reaction at 500°C may be a consequence of this reductive fragmentation process, which will result in lower *N* values.

With reference to the unpromoted catalyst, the action of potassium on iron oxide in the industrial catalyst is probably two-fold: firstly, it increases the activity of the catalyst by increasing the concentration of surface labile oxide anions, although their origin may be different. Here, the activated species may be formed from the interaction of potassium species with the oxide forming an Fe^{n+}–O–K^{n+} species on the catalyst surface. The stoichiometry of

this species is maintained by steam. This suggestion is supported by the study of Coulter et al. [12] where they found that the optimal molar ratio of K:Fe on the surface is approximately 1:1. As we have found for MCM-41-supported FeO, this type of surface species also exist in a disordered state as mentioned in Section 1. Obviously, we only consider the effect of potassium on the surface of iron oxide. However, subsurface substitution of potassium will also give rise to the same effect. Secondly, the potassium species might lower the overall cationic charge on iron centers and this decreases their binding strength for the primary product (styrene). The enhanced desorption of surface styrene will minimize its secondary reaction to side products, and thus, improves its selectivity in the observed product.

We have not included the effect of coke formation in these discussions since the amount of carbon formed on the catalyst surface is not large. It should be mentioned that, throughout the process of ethylbenzene dehydrogenation, we do not observe any peak which can be assigned unambiguously to Fe–C bonding as a result of interaction between ethylbenzene and iron oxide.

5. Conclusion

We have demonstrated with X-ray absorption techniques that the structure of iron oxide evolves during catalyst pretreatment and ethylbenzene dehydrogenation reaction. The evolution process initiates in the catalyst pretreatment stages via reduction of the initially formed α-Fe_2O_3 in the as-synthesized catalyst. At 500°C, tetragonally distorted FeO is formed on the surface of MCM-41. The stability of FeO at this temperature comes from the formation of Fe–O–Si linkages with MCM-41 silanol groups. Possibly, one major advantage of stabilizing the FeO structure is to prevent sintering of this species. Without the interfering effect of promoters and steam, the nature of the active center on iron oxide which is responsible for the dehydrogenation of ethylbenzene is easily identified as the activated or labile surface lattice oxygen. There will be a continuous supply of this reactive species for the ethylbenzene dehydrogenation reaction whenever cationic vacancies are present in iron oxide. The concentration of this species diminished when these vacancies were filled and the catalyst deactivated. However, if the iron oxide particles are large, fragmentation can occur and new active materials are formed. We have shown that reductive fragmentation of iron oxide particles occurs in the initial stages of the ethylbenzene dehydrogenation reaction, which causes fluctuation in the activity profile.

Based on our catalytic and X-ray absorption results, we proposed that the ethylbenzene dehydrogenation reaction occurs via a combination of oxidative (initial stages) and non-oxidative (steady stages) mechanisms. The latter comes into play only at longer time on stream.

Acknowledgements

We thank Prof. S.B. Liu of Academia Sinica for allowing us to use his catalytic reaction system and Prof. B.-Z. Wan for his support of this work. This research was supported by the China Petroleum Co. and the National Science Council of Taiwan (NSC 85-2113-31-M-002-032 cc).

References

[1] F. Zaera, A.J. Gellman, G.A. Somorjai, Acc. Chem. Res. 19 (1986) 24.
[2] R. Imbihl, M.P. Cox, G. Ertl, J. Chem. Phys. 84 (1986) 3519.
[3] T. Wang, C. Lee, L.D. Schmidt, Surf. Sci. 163 (1985) 181.
[4] H.F.J. Van't Blik, J.B.A.D. Van Zon, T. Huizinger, J.C. Vis, D.C. Koningsnerger, R. Prins, J. Phys. Chem. 87 (1983) 2264.
[5] M. Nishimura, K. Asakura, Y. Iwasawa, in: Proc. 9th Int. Congr. Catal., Calgary, Vol. 4, 1988, p. 1842.
[6] J.C.J. Bart, Adv. Catal. 34 (1986) 203.
[7] J.C.J. Bart, G. Vlaic, Adv. Catal. 35 (1987) 1.
[8] M. Muhler, J. Schütze, M. Wesemann, T. Rayment, A. Dent, R. Schlögl, G. Ertl, J. Catal. 126 (1990) 339.
[9] T. Hirano, Appl. Catal. 26 (1986) 81.
[10] J. Koppe, I. Rapthel, P. Kraak, Chem. Tech. (Leipzig) 40 (1988) 81.
[11] W.P. Addiego, C.A. Estrada, M.P. Rosynek, D.W. Goodman, R.G. Moore, J. Catal. 146 (1994) 407.
[12] K. Coulter, D.W. Goodman, R.G. Moore, Catal. Lett. 31 (1995) 1.
[13] E.H. Lee, Catal. Rev. 8 (1973) 285.
[14] J.S. Beck, J.C. Vartuli, W.J. Roth, M.E. Leonowicz, C.T. Kresge, K.D. Schmitt, C.T.-W. Chu, D.H. Olson, E.W. Sheppard, S.B. McCullen, J.B. Higgins, J.L. Schlenker, J. Am. Chem. Soc. 114 (1992) 10834.
[15] R. Burch, N.A. Cruise, D. Gleeson, S.C. Tsang, J. Mater. Chem. 8 (1998) 227.

[16] S.T. Wong, H.P. Lin, C.Y. Mou, Appl. Catal. A, accepted for publication.
[17] H.P. Lin, S. Cheng, C.Y. Mou, Microporous Mater. 10 (1997) 111.
[18] J.-H. Choy, J.-B. Yoon, D.-K. Kim, S.-H. Hwang, Inorg. Chem. 34 (1995) 6524.
[19] G. Sankar, P.R. Sarode, C.N.R. Rao, Chem. Phys. 76 (1983) 435.
[20] T. Yokoyama, K. Asakura, Y. Iwasawa, H. Kuroda, J. Phys. Chem. 93 (1989) 8323.
[21] A.N. Shmakov, G.N. Kryukova, S.V. Tsybulya, A.L. Chuvilin, L.P. Solovyeva, J. Appl. Cryst. 28 (1995) 141.
[22] C. Greaves, J. Solid State Chem. 49 (1983) 325.
[23] L.A. Grunes, Phys. Rev. B 27 (1983) 2111.
[24] J.E. Hahn, R.A. Scott, K.O. Hodgson, S. Doniach, S.R. Desjardins, E.I. Solomon, Chem. Phys. Lett. 88 (1982) 595.
[25] C. Brouder, J. Phys.: Condens. Matter 2 (1990) 701.
[26] L.W. Finger, R.M. Hazen, J. Appl. Phys. 51 (1980) 5362.
[27] U. Müller, Inorganic Structural Chemistry, Wiley, New York, 1993.
[28] W. Hückel, Structural Chemistry of Inorganic Compounds, Vol. 2, Elsevier, Amsterdam, 1951.
[29] Y. Kou, Z. Suo, J. Niu, W. Zhang, H. Wang, Catal. Lett. 35 (1995) 279.
[30] Z. Gao, B. Zhang, J. Cui, Appl. Catal. 72 (1991) 331.
[31] A.F. Wells, Structural Inorganic Chemistry, 5th Edition, Clarendon Press, Oxford, 1984.
[32] K. Sakata, F. Ueda, M. Misono, Y. Yoneda, Bull. Chem. Soc. Jpn. 53 (1980) 324.
[33] V.S. Smentkowski, J.T. Yates Jr., Surf. Sci. 232 (1990) 113.
[34] K. Kishi, Surf. Sci. 192 (1987) 210.
[35] A. Koizumi, H. Maeda, N. Bamba, H. Maruyama, E. Takayama-Muromachi, J. Shi, K. Shimizu, M. Mino, H. Yamazaki, Jpn. J. Appl. Phys. 28 (1989) L203.
[36] A.R. West, Solid State Chemistry and its Applications, Wiley, Singapore, 1989.
[37] G. Busca, V. Lorenzelli, G. Ramis, R.J. Willey, Langmuir 9 (1993) 1492.
[38] P. Berthet, J. Berthon, F. d'Yvoire, Mater. Res. Bull. 24 (1989) 459.
[39] M. Misono, K. Sakata, F. Ueda, Y. Nozawa, Y. Yoneda, Bull. Chem. Soc. Jpn. 53 (1980) 648.
[40] N.J. Jebarathinam, M. Eswaramoorthy, V. Krishnasamy, Appl. Catal. 145 (1996) 57.
[41] J. Chen, D. He, S. Cao, Chem. J. Chin. Univ. 7 (1986) 1020.